METHODS FOR COMPENSATING THERMAL MODE DISTORTIONS IN HIGH AVERAGE POWER CHIRPED PULSE AMPLIFIERS

Joshua E. Schoenly[1]

Department of Chemistry and Physics, Saint Michael's College, Colchester, VT 05439

David H. Reitze[2], Vidya Ramanathan, and Jinho Lee

Physics Department, University of Florida, Gainesville, FL 32611

Abstract

Further development of a solid state, high average power, chirped pulse amplifier is presented. The design of a container filled with an optical gel, OCF-446, with a negative dn/dT to compensate for thermal lensing effects in the amplifier is discussed along with designs of a thermoelectric cooling system for the solid state Ti:sapphire crystal in the amplifier. The container is a variable width cell which has a step size of .026 mm / 15^{o} and prevents the OCF-446 from becoming dirty. Experimentation on this cell verifies that OCF-446 acts as a negative thermal lens when it comes in contact with a laser beam. Testing also concludes that a larger path length within the variable width cell leads to an increase in the beam waist. Thus the tunability of the cell's effect on negative thermal lensing is shown to be successful since previous designs were static in path length.

[1] Email: jschoenly@smcvt.edu
[2] Email: reitze@phys.ufl.edu

1. Introduction

The development of high-energy, high-repetition rate solid-state lasers (HHSS) continues to be of interest for both scientists and engineers alike. Countless applications engender HHSS lasers ranging from kinetic chemical analysis of short-lifetime systems to ultrafast surface science to laser synchrotron experiments. Since the development of the first solid-state laser, a ruby laser designed and created by Theodore Maiman operating at a wavelength of 694.3 nm, the progress of solid-state laser engineering has certainly expanded with high energy, high repetition rate lasers reaching an average 13 W of power and 24-fs-duration pulses [1, 2].

Recent solid-state laser engineering has employed the use of amplification designs where a beam of femtosecond pulsed light is stretched to picosecond pulses, amplified in energy, and compressed back into femtosecond pulses. This type of pulse stretching/compressing amplification is commonly called a CPA (chirped pulse amplifier).

The development of HHSS lasers using CPAs for amplification does not come without difficulties. Inherent in high-power lasers is a thermal effect, due to pumping a Ti:sapphire crystal at 80 W and 10 kHz repetition rate. The pump beam heats the crystal thus changing its refractive index. Due to the intensity profile of the beam, each part of the crystal experiences a different change in temperature and thus a different refractive index. An optical path length difference occurs across the crystal thus causing an effect similar to a lens [4, 5, 6].

Thermal lensing significantly affects the output power of the laser beam and, if not corrected for, renders the amplifier output power nearly insignificant at high pump powers due to loss of power into higher order modes caused by thermal lensing. Hence, a procedure to eliminate or compensate for these effects is needed. One such procedure is used in our lab where we have attempted to reduce thermal lensing at the crystal by immersing the crystal in cryogenic temperatures (≈ 77 K). As the temperature of the Ti:sapphire crystal decreases, the thermal conductivity has been observed to increase to an optimum at a temperature of ≈ 25 K. An Optics Letter by Backus reports a cryogenically cooled CPA lasing system

where a minimum temperature of 77 K was reached and little to no thermal lensing effects were observed [2].

We have reached cryogenic temperatures of ≈ 90 K and observed a reduction in thermal lensing. Cryogenic cooling, however, has become costly and time-consuming where full days are often spent trying to maximize the ability of our cooling. Thermal lensing, also, is still apparent in our cryogenic setup when pump powers are increased thus decreasing the focal length of the thermal lens. Our lab has therefore decided to employ a new technique, which will compensate for the thermal lensing effect without cooling the Ti:sapphire crystal to cryogenic temperatures (≈ 77 K). A compensating element (CE) has therefore been used, which, in effect, will refocus the thermal lensing induced defocused laser beam.

The CE used is an optical index-matching fluid OCF-446, which is a clear, colorless, organic liquid with a viscosity comparable to vegetable oil. Past designs of a cell to house the CE were static in path length and saw burning of the OCF-446 on the inside of the cell. Typical cuvettes for fluorescence and UV-*vis* experimentation could also not be used since theoretical simulations by Jinho Lee and an Optics Letter by Th. Graf conclude that a path length of ≈ .3 – 1 mm as the optimum distance whereas most cuvettes are 1 cm in path length [5]. A variable CE chamber has therefore been designed and machined with path lengths ranging from .1 mm – ≈ 1 cm and a step-size of ≈ .026 mm/ 15^{o}. Thermal lensing data obtained by verifying the negative thermal lens induced by the CE are tabulated later in this paper.

Included in this paper as well are designs for a thermoelectrically cooled (TEC) Ti:sapphire holder and vacuum canister which will be later employed into the amplifier cavity to replace the cryogenic cavity. In this case, the heat equation has been approximated for a cylindrical, brewster-cut Ti:sapphire crystal in the TEC cell using the program FEMLAB (a finite element analysis program) so as to clearly observe the temperature difference within the crystal. The TEC will be implemented so the crystal does not reach its damage threshold upon high-power pumping or thermally expand significantly.

It has already been shown in a recent Optics Letter by Zhavoronokov that a TEC system was able to cool the Ti:sapphire crystal to 210 K at no pump power [7]. Future construction of the amplifier cavity, assuming the CE compensates the thermal lensing effects, consists of replacing the current cryogenic system with a TEC system and attempting to reach moderately low temperatures (≥ 210 K).

2. Background

2.1 Chirped Pulse Amplification

Oscillator

The creation of a chirped pulse is achieved by first seeding a pulse stretcher with a self mode-locked wave train of laser light from an oscillator. The pulse widths produced by the oscillator are on the order of 20 fs at a repetition rate of 88 MHz with 300-400 mW of power. A Ti:sapphire crystal is usually employed as the solid-state laser medium of choice since it has a natural optical Kerr effect, which creates femtosecond pulses and is frequency tunable [3].

Stretcher

Pulse seeds enter the stretcher where their pulse widths are increased by an order of 10,000 to a width of 200 ps. The process that occurs within the stretcher is positive chromatic dispersion by a grating of the seed beam where the longer wavelength beams are diffracted at a longer distance than the shorter wavelength beams.

Amplifier

After passing through the stretcher, the laser beam enters the amplifier where a Ti:sapphire crystal is pumped via a high-power, frequency doubled, diode pumped Nd:YAG laser at ≈ 532 nm. The optical layout for the amplifier is shown in Fig. 1.

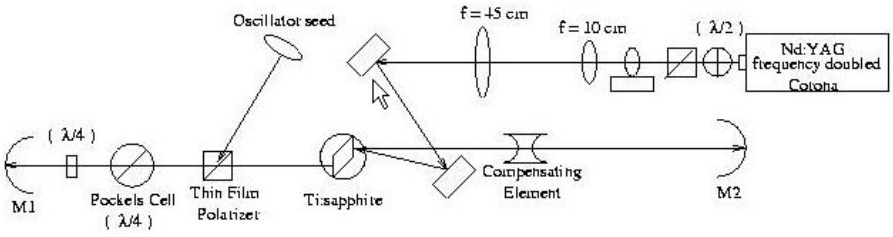

FIGURE 1. Optical layout for our amplifier cavity, i.e. the regenerative amplifier “regen”.

As can be seen in Fig. 1, the pump beam from the Nd:YAG is first focused tightly using a 4 cm lens. This focused spot is then imaged on the crystal while being magnified 4.5 times by a telescope such that the intensity of the pump beam does not exceed the damage threshold of Ti:sapphire crystal. The cavity contains two spherical mirrors (i.e. M1 and M2) at either end of the cavity.

The oscillator seed beam enters the amplifier cavity by reflecting off a thin film polarizer, which transmits p-polarized light and reflects s-polarized.[3] Since the seed beam is s-polarized, all of the beam will be reflected into the cavity. For the first pass, the Pockel's cell is turned off so that, as the beam propagates through the cavity, the beam will experience a rotation of its polarization by 90^o as it passes twice through the wave-plate at the left end of the cavity. The beam has become p-polarized and will pass through the crystal to the right end of the cavity. After one complete cavity trip, the Pockel's cell is turned on. The net rotation of the Pockel's cell and the wave plate for a round trip is 180^o, thus keeping a p-polarization within the cavity. After approximately 20 round trips, the Pockels cell is turned off, the pulse polarization rotates to s-polarization, and is ejected from the cavity by the thin film polarizer.

Compressor

The pulse compressor consists of two parallel diffraction gratings and works upon the principle of negative dispersion. The compressor will compress the amplified light pulses back into femtosecond pulses.

2.2 Gaussian Wave Optics

Since light is an electromagnetic wave, Maxwell's equations can be solved in order to find a wave equation for the light beam. Such a derivation is common in many texts on lasers and will not be repeated here; the answers for such a derivation contain a Gaussian parameter and Hermite polynomial [1, 4, 8]. The equation for the beam waist divergence, however, is found in the solutions for the wave equation and is given in Eq. (1) [1].

[3] By convention, p stands for light polarized parallel to the optics table while s is perpendicularly polarized.

$$w(z)^2 = w_0^2\left[1+\left(\frac{z}{z_0}\right)^2\right] \tag{1}$$

In Eq. (1) the beam waist *w* is a function of the longitudinal displacement along the z axis, w_0 is the minimum beam waist at z = 0, and z_0 is the Raleigh range by Eq. (2) [1].

$$z_0 = \frac{\pi n w_0^2}{\lambda_0} \tag{2}$$

In Eq. (2), the wavelength of the light beam is λ_0 and the refractive index of the propagation medium is n. According to Eq. (2), z_0 is defined as the longitudinal distance the beam travels to increase its minimum beam waist by $\sqrt{2}$. Fig. 2 incorporates Hermite-Gaussian waves into a resonating cavity with two spherical mirrors.

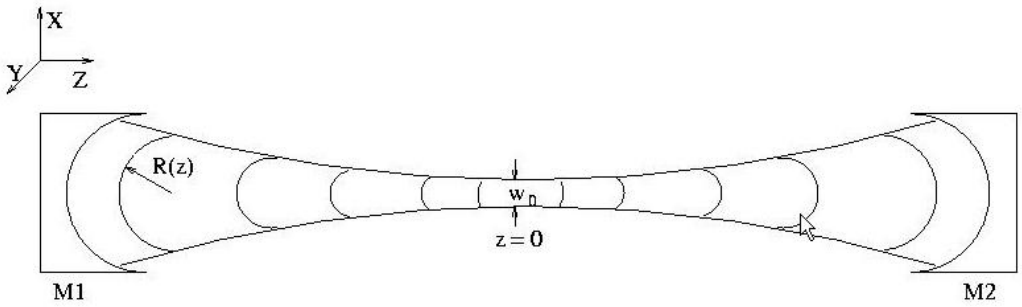

FIGURE 2. Gaussian beam resonating within a cavity. The spherical mirrors, M1 and M2, are selected such that the radius of curvature of the Gaussian beam R(z) is the same as the curvature of the mirrors when the beam impinges upon their surface. When z = 0, the beam waist is at its minimum w_0.

The radius of curvature of the Gaussian wave R(z) is given by Eq. (3) which is also found in the solutions for the Maxwell wave equation [1]. As can be seen in Eq. (3), as z approaches zero, the radius of curvature of the beam becomes infinite which concludes that when *w* equals w_0, the beam is flat.

$$R(z) = z\left[1+\left(\frac{z_0}{z}\right)^2\right] \tag{3}$$

Since the solutions to Maxwell's wave equation contain both Gaussian and Hermite polynomial parameters, one can expect that a perfect Gaussian beam in both the x and y intensity plane is only one of many solutions. This solution is named the $TEM_{0,0}$ mode. The initials in this mode notation stand for transverse electromagnetic wave, and the numbers stand for the order of the Hermite polynomial in the x and y directions. The intensity profile for varying modes is found in Fig. 3. Also found in Fig. 3 are the intensity profiles looking down upon the transverse axes.

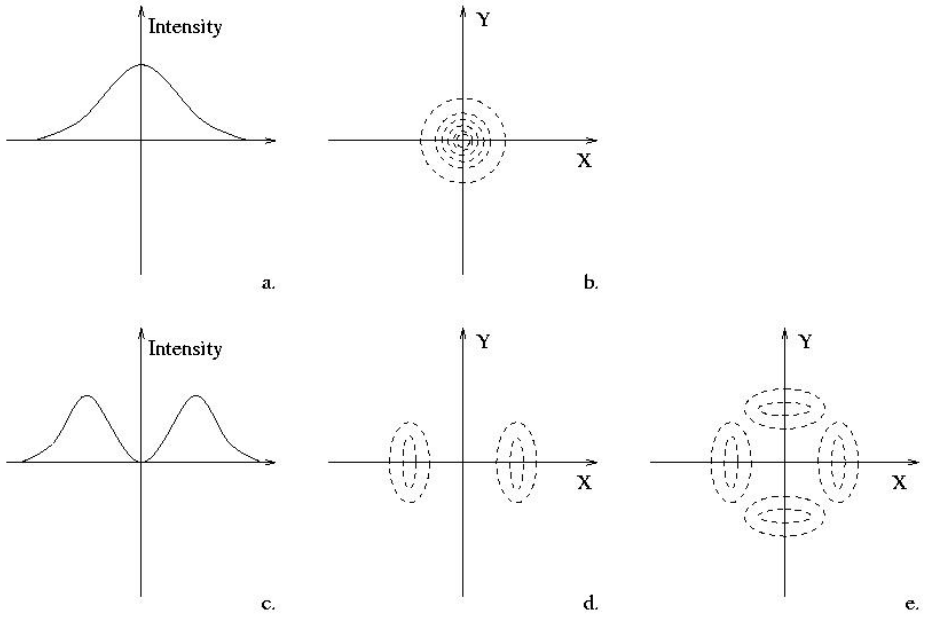

FIGURE 3. Various sketches of Hermite-Gaussian mode intensity profiles along specified axes. The two left most graphs (a and c) show the modes' intensity as a function of one transverse direction. The graphs to the right (b, d, and e) look down the intensity axis upon the xy plane. Fig. 3b relates the $TEM_{0,0}$ mode where both the x and y axes are representative of the intensity plot found in a. In Fig. 3d, the y-axis intensity is representative of a but the x axis is representative of c. The mode in Fig. 3d is termed $TEM_{0,1}$. A $TEM_{1,1}$ mode is seen in Fig. 3e, where both the x and y axes are representative of c.

2.3 Thermal Lensing

Thermal lensing is a thermally induced optical distortion effect, which occurs when a high power laser beam is incident upon a material of initial refractive index n_0. The refractive index of the material is not a constant quantity since it varies with material temperature, internal stresses, wavelengths, and polarization of light. If a high-energy laser beam pumps a crystal within a solid-state laser, there will be a

large temperature increase within the crystal. For most solid-state lasers, temperature dependence of the refractive index dominates thermal lensing effects [6]. The refractive index *n(T)* at the final temperature can be found by expanding around T_i using a Taylor Series expansion, as seen in Eq. (4) [4].

$$n(T) = n_0(T_i) + \Delta T \frac{\partial n}{\partial T}\Big|_{T=T_i} + \Delta T^2 \frac{\partial^2 n}{\partial T^2}\Big|_{T=T_i} + \ldots \tag{4}$$

In Eq. (4), $\Delta T = (T - T_i)$ is the change in temperature of the crystal, and $\frac{\partial^j n}{\partial T^j}\Big|_{T=T_i}$ is the jth partial derivative of the refractive index evaluated at T_i. Typically the higher order terms in Eq. (4) are small compared to the first order terms and can be ignored. If the input beam is assumed to be in the $TEM_{0,0}$ mode, the most intense portion of the input beam will be in the center. Thus, if the input beam is aimed at the center of a cylindrically shaped crystal, the center of the crystal will have the largest increase in temperature to about 600 K as seen in Fig. 4. Therefore, there will be different refractive indices on and

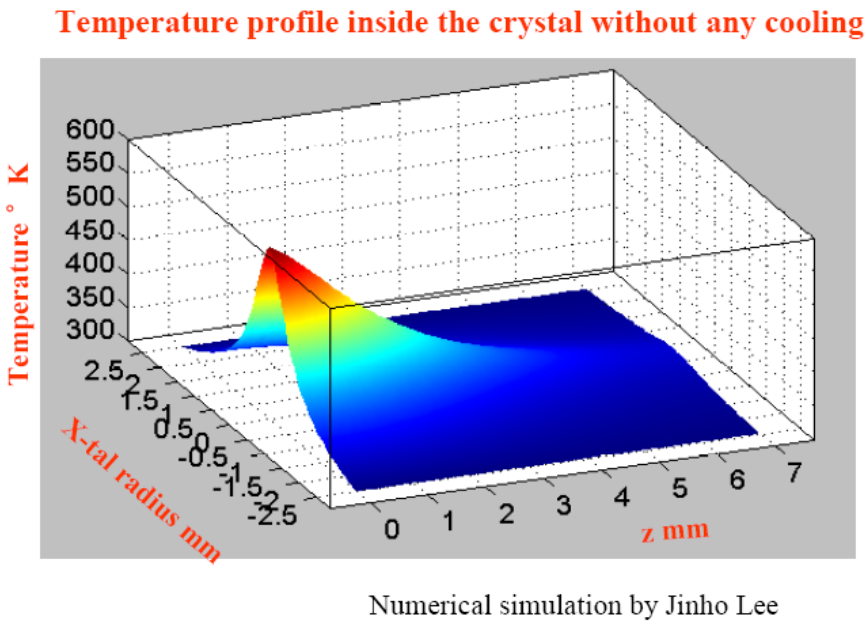

FIGURE 4. Temperature profile at 80 W of pumping within a Ti:sapphire without cooling. Temperatures rise to 600 K without cooling at the center of the crystal thus giving rise to significant thermal lensing.

throughout the crystal depending upon the distance r from the center axis of the crystal. In effect, a convex lens will form, thus focusing the light at a distant focal length. W. Clarkson has used a thin film approximation of a continuously pumped, cylindrical media to determine the thermally induced focal length f_{th}, given in Eq. (5), by estimating the lens created is symmetrically spherical in curvature [6].

$$f_{th}(r) = \frac{2\pi K_c r^2}{P_p \gamma \eta_{abs} (dn/dT) s(r)} \tag{5}$$

In Eq. (6), K_c is the thermal conductivity of the crystal, P_p is the incident pump power, γ is the fraction of pump power absorbed dissipated as heat, η_{abs} is the fraction of the pump power absorbed in the laser rod, and $s(r)$ is the fraction of pump power contained within a disc of radius r and intensity profile I_P given by Eq. (6) [6].

$$s(r) = \frac{2\pi}{P_p} \int_0^r r' I_p(r') dr' \tag{6}$$

For the thermal lensing effect to be made as small as possible, f_{th} must be a large number to induce a negligible divergence from the cavity. One solution is to raise the thermal conductivity by lowering the temperature of the crystal. In Fig. 6, we see that the thermal conductivity of sapphire has a maximum at ≈ 25 K. With such a large increase in thermal conductivity, a cryogenic setup has been used to significantly reduce thermal lensing [2].

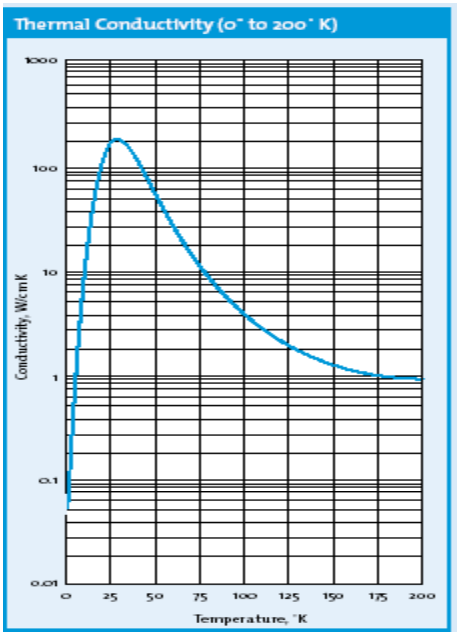

FIGURE 5. Thermal conductivity of sapphire vs. temperature. The maximum thermal conductivity of sapphire reaches a maximum at ≈ 25 K [9].

We have used Eq. (5) to determine the focal length of the thermal lens at 77 K and 300 K with a pump beam at 70 W and 10 kHz. The focal lengths differ by about a factor of 10 where the focal length at 300 K is f_{th} = 5.6 cm while at 77 K f_{th} = 45.5 cm. Hence, there is a significant decrease in thermal lensing as one decreases the temperature of the Ti:sapphire crystal.

An alternative solution is to introduce a negative/concave lens of the same magnitude as f_{th} within the cavity as seen in Fig. 6. However, this lens must be dynamic and be able to adjust its lens as the pump power changes. Therefore, a material of negative (dn/dT) should be introduced within the cavity to dynamically change along with the power of the laser.

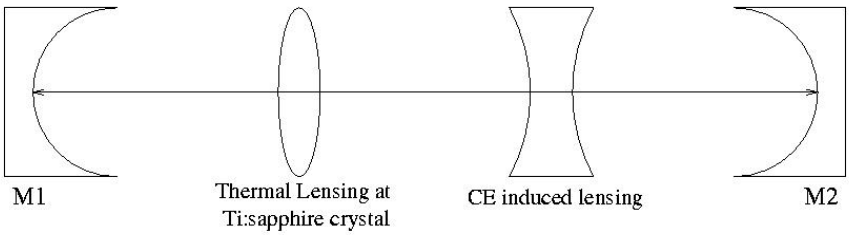

FIGURE 6. Compensation of the positive lensing at the Ti:sapphire crystal using a CE

3. Design Schematics

3.1 Compensating Element Variable Width Cell

Thermal lensing effects have been significantly reduced using a cryogenic setup, however, the compensation of the cryogenic setup also decreases as one increases the power of the pump beam as seen in Fig. 7. In Fig. 7, one can see that for every watt increase from the pump beam leads to an increase in 1.5 ^{o}C. Hence, at half the pump power, the temperature of the crystal has already decreased to ≈ -115 ^{o}C. The upkeep of the cryogenic system has become cumbersome as well with purchasing liquid nitrogen and waiting a long time for the crystal to heat up to fix anything within the evacuated cavity.

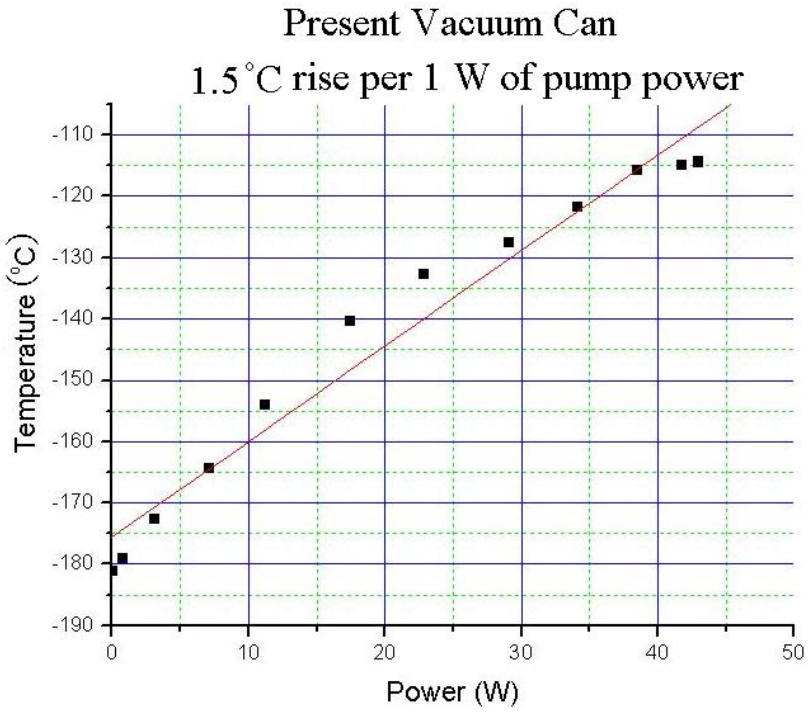

FIGURE 7. Temperature increase in the Ti:sapphire crystal as a function of pump power. An increase in the pump power by one watt in our amplifier increases the temperature of the crystal by one and a half-degree Celsius.

An easier method to compensate for the positive lens induced at the crystal is to introduce a compensating element (CE) which has a negatively induced lens. A CE is typically a liquid because liquids usually have a negative (dn/dT). A previous optics letter by Th. Graf details an experiment

where the optical gel OCF-446 is used in conjunction with a high power laser to decrease thermal lensing effects [5]. Previous designs for a cell to house OCF-446 lacked path length variability thus restricting their operation to fixed path lengths.

We therefore have designed and machined a variable path length cell to house the OCF-446. The design for this cell is shown in Fig. 8. The chamber at the top of the cell holds the excess OCF-446 when the liquid is not in the cell. The cell operates by rotating the right piece in the left drawing into the left piece. The distance between windows of the cell goes from ≈ 1 cm down to .025 mm. Notches on the outside of the cell give a window path movement of .026 mm per 15^{o} rotation. The windows were ordered from CVI laser and are parallel with an uncertainty of > 10 arcsec.

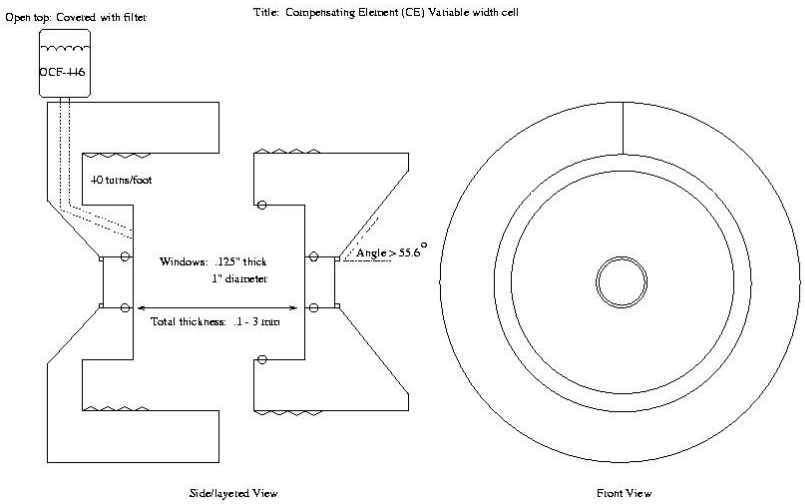

FIGURE 8. Design schematic for a compensating element variable width cell. The circles in the left picture represent o-rings to prevent leakage from the cell. The right component in the side/layered view has an entrance angle of $>55.6^{o}$, the approximate Brewster angle for OCF-446 and the windows.

Before the cell was used in experimentation, it was first tested to accrue knowledge about its operation. The first two attempts to fill the cell were unsuccessful because some of the OCF-446 had leaked into the screw pitches upon turning the cell rendering any attempts to rotate the cell nearly impossible. The leakage was attributed to excess lubrication of the interlocking o-ring between the two

pieces, thus filling the smaller piece of the cell with more OCF-446 than necessary. A third attempt turned out to be successful since we tested the cell with a vegetable oil based lubricant. The optimum way to fill the cell, it was found, was to bring the windows to a minimum distance, fill the chamber with OCF-446, and start rotating outwards.

3.2 Thermoelectrically cooled Ti:sapphire holder

Provided the CE cell compensates thermal lensing effects within the regen cavity, a cooling apparatus for the Ti:sapphire crystal will be still necessary to prevent excessive thermal expansion of the crystal and the crystal exceeding its damage threshold. Since achieving cryogenic temperatures will not be necessary, a new system will be built which will be cheaper and easier to work with than the cryogenic setup. The cooling apparatus that has been considered is a thermoelectric cooler (TEC) which works on the principle of the Peltier effect. The Peltier effect concerns the movement of electrons from one side of the TEC to the other. On one side of the TEC, the electrons will absorb thermal energy thus making one side cool. The opposite will occur on the opposite side of the TEC where electrons will release thermal energy thus heating that side. The cool side will be applied nearest to the crystal while the other side is applied nearest to a heat well to prevent an excessive buildup of heat and damage to the TEC. A prototype TEC holder for the Ti:sapphire crystal has been designed and can be seen in Fig. 9.

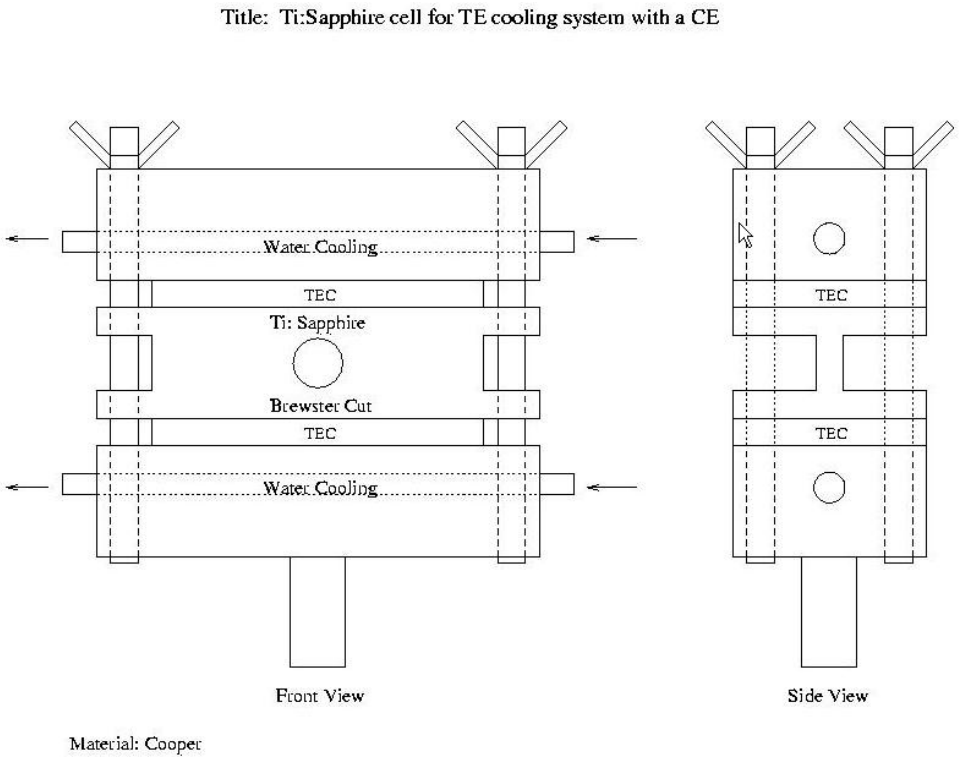

FIGURE 9. Design schematic for the Ti:sapphire holder with a TEC. Four metal poles with wing nuts on the top will keep the holder tightly together. The hot side of the TEC is closest to a water-cooling pipe which has cool water provided externally.

The TEC holder, unfortunately, has not been machined since the CE cell has not been tested within the regen cavity due to complications with the Nd:YAG power supply. Provided the CE cell compensates for thermal lensing, the TEC holder will be machined and will be placed, along with the CE cell and another TEC holder, within an evacuated cavity. In the future, our lab hopes to create a double pumping scheme where two YAG lasers pump two Ti:sapphire crystals thus creating a higher amplification. A design for the evacuated cavity, which will house the two TEC holders and the CE cell, is provided in Fig. 10.

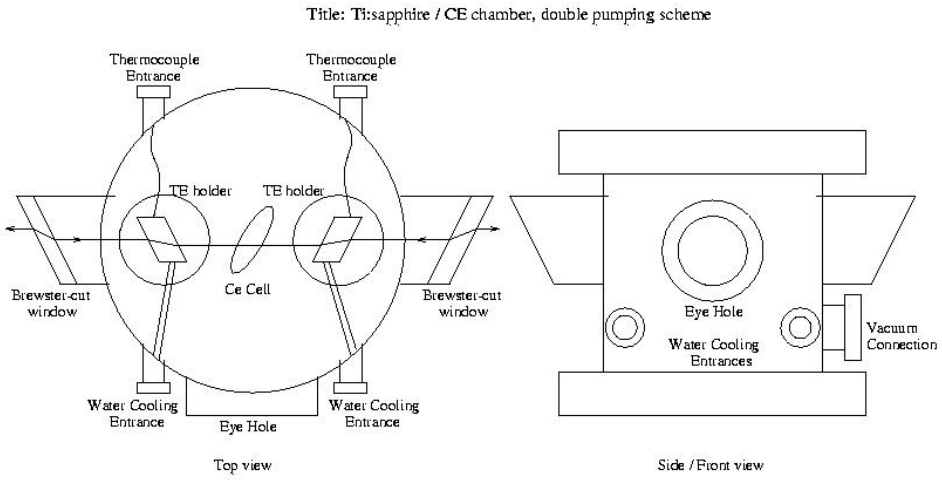

FIGURE. 10. Design schematic for the Ti:sapphire / CE cell evacuated chamber for a double pumping scheme. The CE cell is in an ideal place because the high power pump beam is not buffeting it.

4. Experimentation

4.1 Comparing the cavity waist with and without OCF-446

Method

Since the power supply for the Nd:YAG pumping the amplifier was broken during the last part of the REU program, we were unable to place the CE cell within the regen cavity and compare beam waists at the Ti:sapphire crystal with and without the CE in the cavity. While this particular experiment could not be performed, another experiment was performed using the output laser from the oscillator to observe the divergence effect induced by the CE. In this separate experiment, the oscillator laser was used in which the average output power was ≈ 250 mW. At such a low power output, it was difficult to observe a large divergence effect. A beam scanner was used to measure the beam diameter of the beam's intensity profile. The setup for this experiment is shown in Fig. 11.

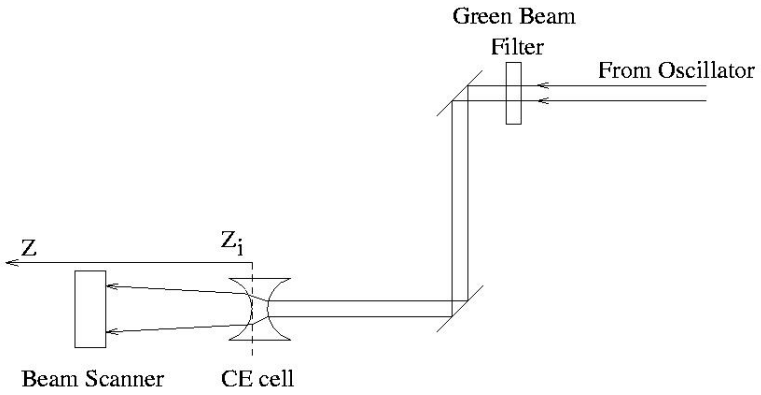

FIGURE. 11. Experimental setup to find the beam waist as a function of z. The constant z_i is the point where $w = w_0$ and is typically unknown when performing the experiment.

In performing this experiment, data were obtained for the beam diameter as the beam scan moved along the positive z-direction. One can, therefore, use Eq. (2) to find w_0 by finding w at various values of z. There is a detail, however, that should not be overlooked. The parameter z is determined by its distance from z = 0 where $w = w_0$, which is not known in the experimental setup. Hence, one must define an arbitrary zero point and modify Eq. (2) to give Eq. (7).

$$w = w_0 \sqrt{\left(1 + \left(\frac{(z - z_i)}{z_0}\right)^2\right)} \tag{7}$$

In Eq. (8), z is now the distance from the arbitrary zero point and z_i is the actual zero point. In order to determine w_0 and z_i, one must now estimate these values that will best fit the experimental data. A program in Matlab had been created previous to this experiment that fits the experimental data to the best curve and thus the best values of w_0 and z_i using Eq. (7).

Results

From the beam waist data at various distances z, we were able to fit a curve to the experimental data by using Eq. (8). These curves can be seen in Fig. 12, where the beam waist of the input laser beam is found on both the horizontal and vertical axes.

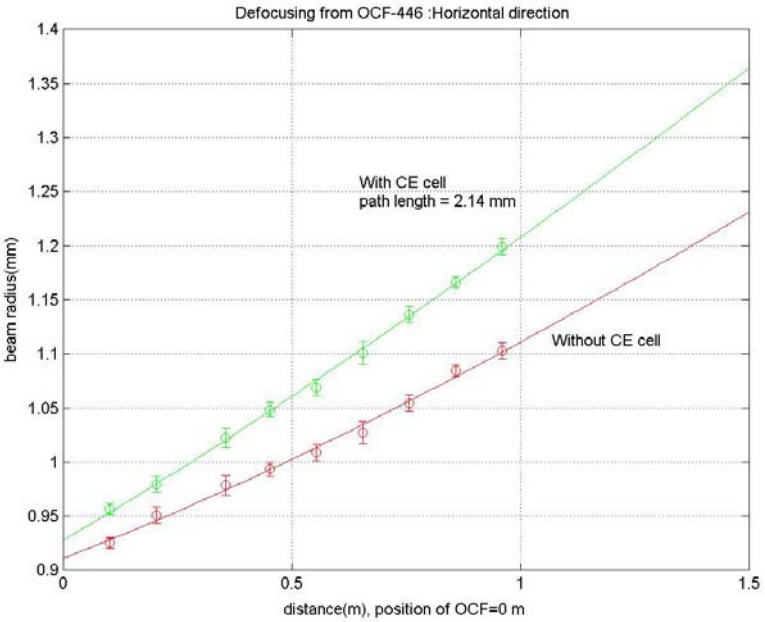

(a) Horizontal component of pump beam.

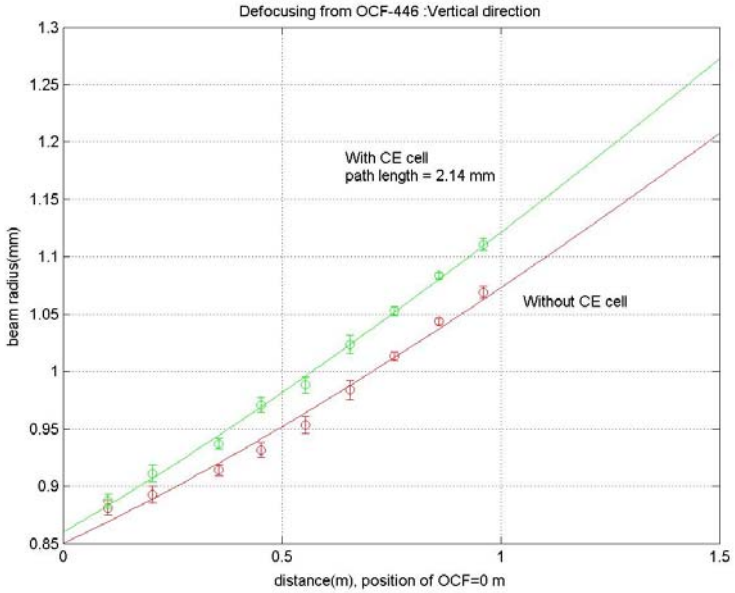

(b) Vertical component of the pump beam

FIGURE. 12. Beam waist data for both the horizontal (a) and vertical (b) axes. In both graphs, inclusion of the CE cell leads to more divergence of the pump beam.

Fig. 12 shows the beam waist diverges more rapidly when the input beam impinges upon the CE cell. What can also be observed is that the beam waist along the horizontal axis diverges more rapidly than the beam waist along the vertical axis. This can be explained by stating that the CE cell is placed at Brewster's angle for OCF-446, which is $\approx 55.6^{o}$. The beam, therefore, will experience a larger optical path length along the horizontal axis while the beam along the vertical axis will not be changed. Also, the oscillator beam could have been elliptical rather than spherical impinging upon the CE cell.

The focal length of the CE cell can also be determined from the data by using Eq. (4) for the radius of curvature of the beam and Eq. (8) where *f* is the focal length, R_1 is the input beam radius of curvature, and R_2 is the output beam radius of curvature.

$$\frac{1}{f} = \frac{1}{R_1} - \frac{1}{R_2} \tag{8}$$

Focal length data are tabulated in Table I. As can also be seen from this data in Table I, the focal length magnitude for the horizontal axis is approximately two times smaller than the magnitude for the focal length along the vertical axis. This closer focal length thus shows that along the horizon, the beam waist diverges more quickly than along the vertical as was seen in Fig. 12.

TABLE I: Focal length data for Fig. 9.

Axis	F (m)	R_1 (m)	R_2 (m)
Horizontal	-11.4	5.588	3.70
Vertical	-21.9	4.740	3.90

4.2 Determing the beam waist as a function of CE pathlength

Method

We are also interested in how the beam waist changes as a function of the pathlength between the windows of the CE cell. The difference in optical path length ΔOPL is the primary cause of concern in thermal lensing since this value depends upon the refractive index *n(T)* and the change in physical path length of the CE cell Δd and is given in Eq. (9).

$$\Delta OPL \approx n(T) \cdot \Delta d \tag{9}$$

For a large ΔOPL , there will be more divergence of the laser beam. Thus, if Δd is increased than ΔOPL will also increase as given by Eq. (9). Since the refractive index is a function of T, the effect of positive and negative thermal lensing is also seen in Eq. (9) by looking at Eq. (4) for *n(T)*. If there is a large ΔT and if dn/dT is positive, than *n(T)* is large corresponding to a large difference in optical path length. The reverse is true for a negative dn/dT giving a smaller difference in optical path length.

The experiment was setup similar to Fig. 11 except that the beam scan did not move. According to theory in Eq. (9), if the path length between the windows is increased than the divergence should increase as well. The tunability of the CE is also being tested in this experiment since simulations made by Jinho Lee relate the how the path length of the CE cell compensates thermal lensing effects by determining the percentage of the original intensity profile from the output. The graphs for these simulations are given in Fig. 13 and show that has the path lengths increase, more compensation occurs at higher pump powers until the path length is 1.4 mm.

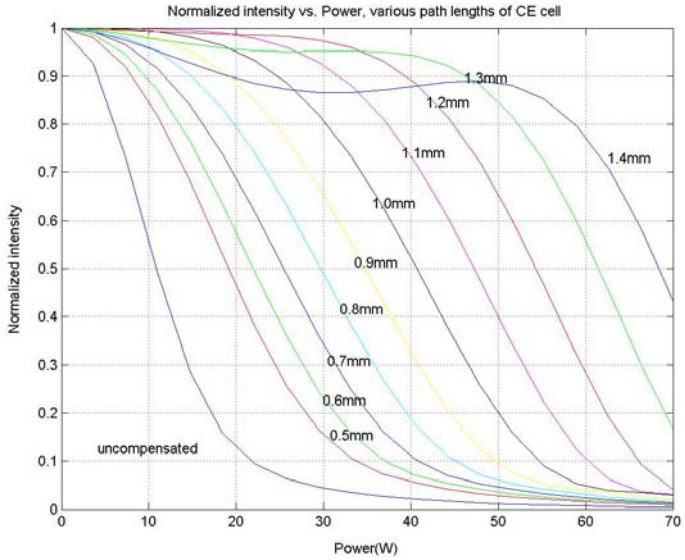

(a) Path lengths from .5 mm – 1.4 mm

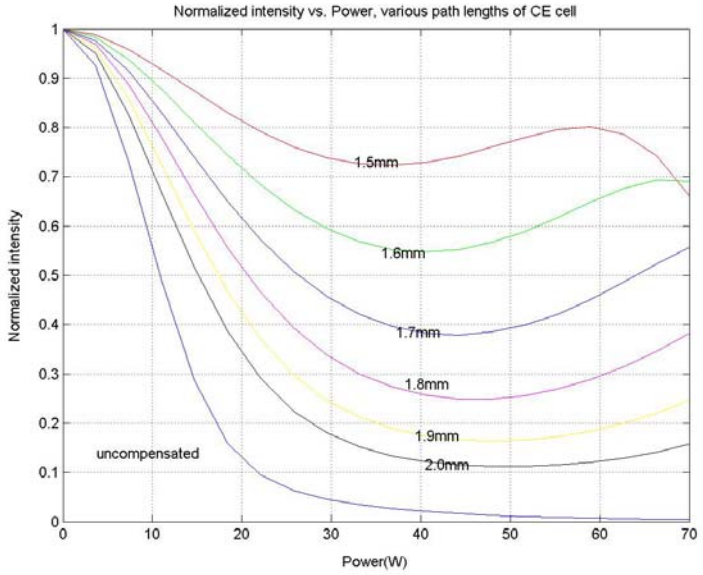

(b) Path lengths from 1.5 mm – 2.0 mm

FIGURE. 13. Compensation of thermal lensing as a function of power for various CE cell path lengths. The normalized intensity is the percentage of the original intensity of the input beam in the output beam. As can be noted in (a), the optimum path length would be either 1.3 mm or 1.4 mm since they do not change the intensity profile of the input beam much at high pump powers

Results

The plotted results of the data are given in Fig. 14 (viewed on page 21). As can be seen in these two graphs, the data tend to show a linear trend of beam diameter vs. CE path length. As proposed by Eq. (9), an increase in the path length between the windows does lead to an increase in beam waist and thus an increase in divergence. Some of the data points, however, do not agree very well with the trend line in Fig. 14. This disagreement is attributed to the changing of the oscillator beam with time since the beam was fairly unstable. This disagreement can also be attributed to the fact that the power of the beam was ≈ 300 mW and thus almost negligible compared to the power levels in an amplifier cavity. The data were therefore difficult to take because there was little negative thermal lensing.

5. Conclusion

Our results verify that OCF-446 creates a divergence of the beam waist of the input beam at even low power (power ≈ 250 mW – 300 mW). The beam divergence corresponds to both the width of the CE cell and the temperature increase of OCF-446 as seen in Eq. (9). The design of the CE variable width cell has proven to be successful since there was no sign of leakage, and the tunability of the width offers a wide range of path lengths from which to test when the CE cell is placed within the regen cavity. We have shown that the beam is able to diverge at a variety of path lengths even at low input power where little thermal lensing occurs. It is unfortunate that we were unable to place the CE cell within the regen cavity, which would have been an optimum experiment for testing the compensation of the OCF-446 and the tunability of the CE cell. This will be accomplished once the laser is prepared.

Our future work is to first cut the sides on the large piece of the CE cell and make a larger entrance angle because it was evident that some light was clipped during our experiment when the cell was set at Brewster's angle. Once the amplifier is operational, we will place the CE cell within the cavity and use a CCD (charge coupled device) camera to measure the spot size on the crystal and mirrors and compare with the spot sizes when the CE cell is not within the cavity. If there is any change in the spot

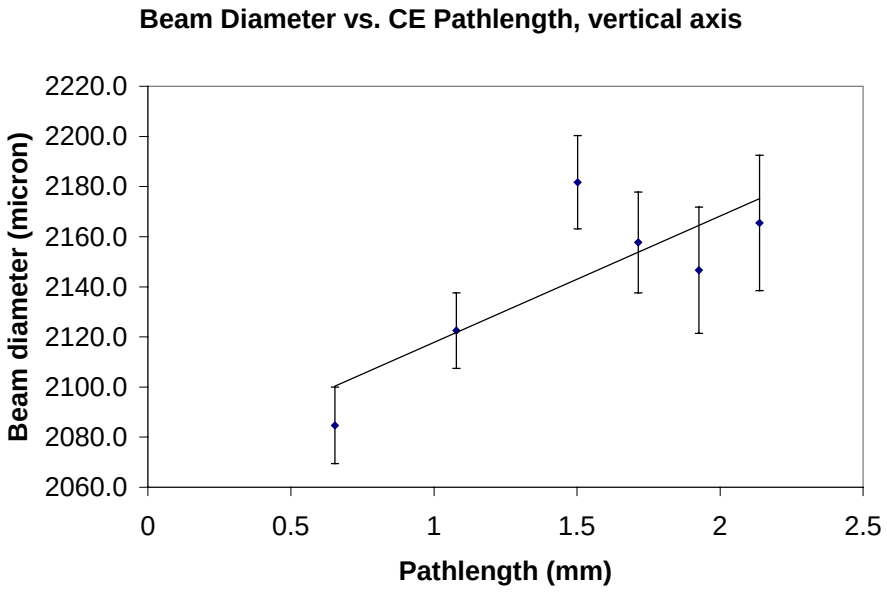

(a) Vertical component of the beam

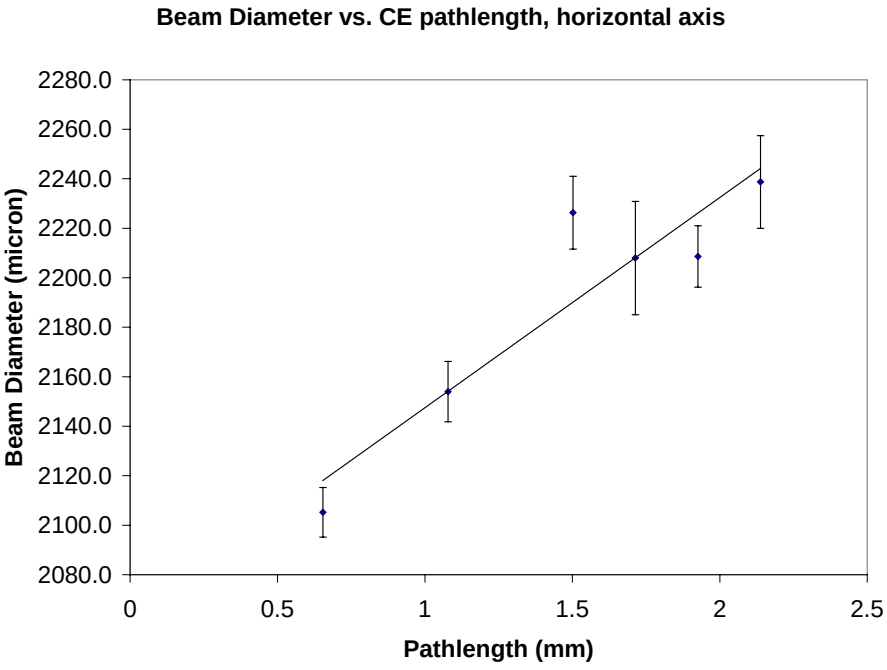

(b) Horizontal component of the beam

FIGURE. 14. Plotted data for beam diameter vs. CE path length. There is an approximate linear trend between path length and beam diameter.

size, we will pursue construction of the TEC holder and chamber, in Fig. 8 and 9, and discontinue use of the cryogenic system.

6. Acknowledgments

I would first like to thank the NSF REU program for funding me in my summer research. I would also like to thank Dr. Reitze for allowing me to work in his lab and offer guidance through these 10 weeks. Many thanks to my coworkers Vidya Ramanathan and Jinho Lee for answering my questions and helping me do my research in the lab. I would also like to thank the coordinators of this program, Dr. Ingersent and Dr. Dorsey, for selecting me to do research at the University of Florida.

7. References

[1] J. Verdeyen, *Laser Electronics*,2nd ed. (Prentice-Hall, New Jersey, 1989).

[2] S. Backus, R. Bartels, S. Thompson, R. Dollinger, H. Kapteyn, and M. Murnane, Opt. Lett. **26**, 465 (2001).

[3] P. Atkins and J. De Paula, *Physical Chemistry*, 7th ed. (W.H. Freeman and Company, New York, 2002).

[4] W. Koechner, *Solid State Laser Engineering*, 5th ed. (Springer, Berlin, 1999).

[5] Th. Graf, E. Wyss, M. Roth, and H. Weber, Opt. Comm. **190**, 327 (2001).

[6] W. Clarkson, J. Phys. D: Appl. Phys. **34**, 2381 (2001).

[7] N. Zhavoronokov and G. Korn, Opt. Lett. **29**, 198 (2004).

[8] A. Siegman, *Lasers* (University Science Books, Sausalito, CA, 1986).

[9] http://www.saphikon.com/qrg.pdf .